Three-dimensional printed bone scaffolds

Citation for published version (APA):
Domingos, M., Gloria, A., Coelho, J. F. J., Da Silva Bartolo, P. J., & Ciurana, J. (2017). Three-dimensional printed bone scaffolds: The role of nano/micro-hydroxyapatite particles on the adhesion and differentiation of human mesenchymal stem cells. *Institution of Mechanical Engineers. Proceedings. Part H: Journal of Engineering in Medicine*. https://doi.org/10.1177/0954411916680236

Published in:
Institution of Mechanical Engineers. Proceedings. Part H: Journal of Engineering in Medicine

Page Proof Instructions and Queries

Greetings, and thank you for publishing with SAGE. We have prepared this page proof for your review. Please respond to each of the below queries by digitally marking this PDF using Adobe Reader (free at https://get.adobe.com/reader).

Please use *only* the circled tools to indicate your requests and responses, as edits via other tools/methods are not compatible with our software. To ask a question or request a formatting change (such as italics), please click the ⟨⟩ tool and then choose "Text Callout." To access the necessary tools, choose "Comment" from the right-side menu.

Sl. No.	Query
	GQ: Please confirm that all author information, including names, affiliations, sequence, and contact details, is correct.
	GQ: Please review the entire document for typographical errors, mathematical errors, and any other necessary corrections; check headings, tables, and figures.
	GQ: Please ensure that you have obtained and enclosed all necessary permissions for the reproduction of artworks (e.g. illustrations, photographs, charts, maps, other visual material, etc.) not owned by yourself. please refer to your publishing agreement for further information.
	GQ: Please note that this proof represents your final opportunity to review your article prior to publication, so please do send all of your changes now.
	GQ: Please confirm that the acknowledgement, funding and conflict of interest statements are accurate.
1	AQ: Please check whether the hierarchy of the section head levels is correct throughout the article.
2	AQ: Please check whether Ref. 25 is correct as set.
3	AQ: Please check whether Ref. 40 is correct as set.

Three-dimensional printed bone scaffolds: The role of nano/micro-hydroxyapatite particles on the adhesion and differentiation of human mesenchymal stem cells

Marco Domingos[1], Antonio Gloria[2], Jorge Coelho[3], Paulo Bartolo[1] and Joaquim Ciurana[4]

Abstract

Bone tissue engineering is strongly dependent on the use of three-dimensional scaffolds that can act as templates to accommodate cells and support tissue ingrowth. Despite its wide application in tissue engineering research, polycaprolactone presents a very limited ability to induce adhesion, proliferation and osteogenic cell differentiation. To overcome some of these limitations, different calcium phosphates, such as hydroxyapatite and tricalcium phosphate, have been employed with relative success. This work investigates the influence of nano-hydroxyapatite and micro-hydroxyapatite (nHA and mHA, respectively) particles on the in vitro biomechanical performance of polycaprolactone/hydroxyapatite scaffolds. Morphological analysis performed with scanning electron microscopy allowed us to confirm the production of polycaprolactone/hydroxyapatite constructs with square interconnected pores of approximately 350 μm and to assess the distribution of hydroxyapatite particles within the polymer matrix. Compression mechanical tests showed an increase in polycaprolactone compressive modulus (E) from 105.5 ± 11.2 to 138.8 ± 12.9 MPa (PCL_nHA) and 217.2 ± 21.8 MPa (PCL_mHA). In comparison to PCL_mHA scaffolds, the addition of nano-hydroxyapatite enhanced the adhesion and viability of human mesenchymal stem cells as confirmed by Alamar Blue assay. In addition, after 14 days of incubation, PCL_nHA scaffolds showed higher levels of alkaline phosphatase activity compared to polycaprolactone or PCL_mHA structures.

Introduction

AQ1

Bone is able to heal and remodel without leaving any scar in cases of very limited damage. However, in pathological fractures, traumatic bone loss or primary tumour resection, where the bone defect exceeds a critical size, bone is no longer able to heal itself.[1,2] In these cases, the clinical approach requires the use of bone grafts, defined as an implanted material that promotes bone healing, alone or in combination with other materials, through osteogenesis, osteoinduction and osteoconduction.[3] Autografts, the gold standard in reconstructing small bone defects, are harvested from one site and implanted into another within the same individual. There is no risk of disease transmission or immune system rejection. Main complications are limited availability, donor-site morbidity and pain, prolonged hospitalization, increased risk of deep infection

[1]School of Mechanical, Aerospace and Civil Engineering, The University of Manchester, Manchester, UK
[2]Institute of Polymers, Composites and Biomaterials, National Research Council of Italy, Naples, Italy
[3]CEMUC, Department of Chemical Engineering, University of Coimbra, Coimbra, Portugal
[4]Universitat de Girona, Girona, Spain

Corresponding author:
Marco Domingos, School of Mechanical, Aerospace and Civil Engineering, The University of Manchester, Manchester M13 9PL, UK.
Email: marco.domingos@manchester.ac.uk; marcod_5@hotmail.com

and haematoma.[2,4] Allografts (natural bone material explanted from a similar donor) could be used as an alternative by reducing site morbidity and pain commonly associated with autografts. However, the risk of immune rejection, transmission of pathogenic diseases and low integration with native tissues clearly reduce their clinical application.[5–11] Synthetic implants, based on metallic or ceramic materials, may be seen as alternative to both autografts and allografts.[5] Despite being able to provide an immediate mechanical support in the area of the defect, restoring the structural stability required for bone healing, metallic implants exhibit a low osteointegration and may increase the risk of bone fracture due to the mechanical properties mismatch. On the other hand, the use of ceramic implants with high capability to promote osteointegration and osteoinduction remain limited due to low torsion, bending and shearing resistance.[5–14] Therefore, strategies based on the combined use of scaffolds, cells and biomolecules are gaining an increasing importance as a viable alternative to the abovementioned clinical therapies.[15] The success of this therapy relies on the ability to generate an adequate biomechanical environment for cellular growth and new tissue formation. The material's requirements used for the production of scaffolds have greatly evolved during the past few years, changing from bioinert to bioactive systems capable of incorporating biomolecules and/or cells hence establishing a more effective interaction with the native tissues.[16,17] Several studies reported the use of polymeric- and ceramic-based materials for the production of bone tissue engineering (TE) scaffolds.[18–21] The most commonly used biodegradable polymers are polycaprolactone (PCL), polylactic acid and polyglycolic acid (PGA) mainly due to their biocompatibility and processability.[22–26] PCL possesses several properties that make it a very attractive material for the production of TE scaffolds, namely, its low biodegradation rate (2–4 years in vivo), high chemical and thermal stability, biocompatibility and low cost.[27–29] Nonetheless, its application in TE remains quite constrained due to its low bioactivity, which limits the integration or mechanical interlock between the implant and the native tissue. To overcome this limitation, researchers have been exploring the introduction of ceramic materials, namely calcium phosphates (CPs), attempting to increase the bioactivity of the produced scaffolds.[30–32] Hydroxyapatite (HA) and tricalcium phosphate (TCP) are inorganic components with a chemical composition very similar to that of the mineral bone phase. This chemical similarity is determinant for the apatite deposition process, protein adsorption and subsequent bone regeneration.[33] The production of biphasic composites (organic–inorganic), mixing polymers and CPs enable us to conjugate the high mechanical performance of polymers with the increased compression resistance of ceramics, hence mimicking the biomechanical properties of bone.[34,35] In general, the results reported in the literature highlight an increment of the mechanical and biological performance of TE scaffolds related with the introduction of CPs.[35–37] However, very few works describe the effect of CPs granulometry on the mechanical behaviour and cellular activity of composite scaffolds.[38,39] Heo et al.[38,39] reported the production and evaluation of nano- and micro-HA composite scaffolds both in vitro and in vivo. Nonetheless, the method used for the preparation of the blends (with organic solvents) and the shape of the particles (irregular) prevent the scalability of the process and the accurate biomechanical evaluation of the structures. Therefore, this article explores the use of a screw-assisted extrusion-based additive manufacturing (AM) system to produce bioactive porous composite scaffolds, consisting of PCL and nano- or micro-HA (nHA and mHA, respectively) particles with regular shape and dimensions. The organic–inorganic composites were obtained using a melt blending process, thus avoiding the use of any organic toxic solvents. The effect of the HA addition as well as particle size on the mechanical performance of three-dimensional (3D) scaffolds was assessed in vitro under static compression. Cell viability and osteogenic differentiation of human mesenchymal stem cells (hMSCs) were assessed using Alamar Blue™ and alkaline phosphatase (ALP), respectively.

Materials and methods

Materials

PCL (CAPA 6500, Mw = 50,000) in the form of pellets was obtained from Perstorp Caprolactones (Cheshire, United Kingdom). Synthetic nHA (particle size ⩽ 200 nm) was purchased from Sigma-Aldrich (Sigma-Aldrich Quimica, S.A. Portugal) and used without further modifications. Synthetic mHA (particle size of $5 \pm 1.0\,\mu m$) was supplied by Fluidinova (nanoXIM HAp 402, Fluidinova, SA, Portugal) and used as received.

Preparation of PCL/HA composite blends

Two types of PCL-based blends were initially prepared using HA powder with different granulometries: nano- and micro-HA (nHA and mHA, respectively) particles. PCL/HA blends (25 wt% of HA content) were prepared by melt blending using a Plastograph® EC (Brabender® GmBH & Co. KG, Germany). First, the HA powder was weighed, placed in a glass recipient and dried in an oven at 100 °C for 2 h. Then, PCL pellets were melted in the Brabender at 100 °C and 40 r/min, during 10 min. Once the PCL was fully melted, the HA powder was added and the mixture was kept in the Brabender for 30 min at 100 °C and 40 r/min, in order to promote a complete homogenization of the composite system. The obtained composite blends were removed from the Brabender and compressed into films, using a hydraulic

Table 1. Process parameters used to fabricate PCL/HA scaffolds.

Process parameters				
DV (mm/s)	ST (μm)	LT (°C)	EP (bar)	SRV (r/min)
10	280	90	5	30

DV: deposition velocity; ST: slice thickness; LT: liquefier temperature; EP: extrusion pressure; SRV: screw rotation velocity.

press. Finally, the films were manually cut into pellets and dried under vacuum during 24 h.

Scaffold design and fabrication

For the fabrication of PCL and PCL/HA scaffolds, a screw-assisted AM system was employed, equipped with an extrusion nozzle of 300 μm. A detailed description of the system, along with the flowchart information required for the fabrication of TE scaffolds, can be found elsewhere.[40–42] Rectangular prisms measuring 30 (length) × 30 (width) × 8 mm (height) were produced employing a single lay-down pattern of 0°/90° and a filament distance (FD) of 750 μm. Process parameters are indicated in Table 1. After fabrication, the obtained 3D constructs were cut into smaller blocks of adequate dimensions for further analysis.

Scaffold morphology

Scanning electron microscopy. Scaffold morphology was carried out using scanning electron microscopy (SEM, FEI Quanta 600F). Top and cross-section images were obtained under low vacuum conditions, 12.5 kV voltage and 0.6 Torr of pressure. Obtained micrographs were used to evaluate structural integrity of the scaffolds, distribution of HA particles, pore spatial distribution and consistency between theoretical and experimental values of pore size (FG) and filament diameter (RW). Energy-dispersive X-ray spectroscopy (EDS) was employed to determine the elementary chemical composition of the scaffold's surface using an Oxford INCAx-sight system.

Micro-computed tomography. Micro-computed tomography (μCT) was performed using a SkyScan 1072 system (Aartselaar, Belgium) employing rotational increments of 0.9° along a total angle of 180°. Cross-sectional as well 3D images of the scaffolds were then reconstructed using SkyScan software as well Image J (National Institute of Health, USA), MIMICS (Materialise, Belgium) and RapidForm (IBUS Technology, Inc., Germany). The obtained micro-tomography results enabled the determination of the scaffold porosity and interconnectivity, calculated based on the following equations

$$Porosity = \frac{Vol_{Pores}}{Vol_{Pores} + Vol_{Scaffold}} \times 100 \quad (1)$$

where Vol_{Pores} corresponds to the total volume occupied by the pores and $Vol_{Scaffold}$ corresponds to the total scaffold volume

$$Interconectivity = \frac{Vol_{Poresinterc}}{Vol_{Poresinterc} + Vol_{PoresClosed}} \times 100 \quad (2)$$

where $Vol_{Poresinterc}$ correspond to the total volume of interconnected pores and $Vol_{PoresClosed}$ correspond to total volume of closed pores (not interconnected).

Mechanical analysis

Compression tests were performed to evaluate the effect of HA on the scaffold mechanical properties. Produced scaffolds were cut into smaller samples of 5.0-mm length (*l*), 5.0-mm width (*w*) and 8-mm height (h_0). All tests were carried out at a rate of 1 mm/min up to a strain value of 0.5 mm/mm, using an INSTRON 5566 testing system. The procedure used to determine the 'apparent' stress (σ) and strain (ε) can be found elsewhere.[38]

Biological analysis

In vitro biological tests were carried out in order to investigate the effect of HA particle size on the viability, adhesion, proliferation and differentiation of bone marrow–derived hMSCs, which were used at passages 4–6 from primary culture. PCL and PCL/HA scaffolds were cut into properly shaped blocks to fit inside cell culture plate wells. The structures were sterilized using 70% ethanol/water solution for 24 h, washed extensively with a phosphate buffer solution (PBS) 0.01 M, pH 7.4, irradiated with UV light during 40 min and finally placed in culture media for 2 h. PCL and PCL/HA scaffolds were then seeded with hMSCs, using a density of 17×10^3 cells/sample. Cell viability and proliferation were evaluated using the Alamar Blue assay as described in previous works.[40,43] The osteogenic differentiation of hMSCs was assessed via ALP measurements following a specific biochemical assay (SensoLyte® pNPP Alkaline Phosphatase Assay Kit). ALP was then normalized against DNA quantity using Quant-iT™ PicoGreen kit. Cell-scaffold constructs were also analysed with a confocal laser scanning microscope (CLSM, Zeiss LSM 510/ConfoCor 2), using rhodamine phalloidin staining for actin filaments to qualitatively investigate cell adhesion and spreading at

7, 14 and 21 days after seeding. Confocal images obtained from all the cell-scaffold constructs were processed with Image J software to assess the cell morphology, using a shape factor defined elsewhere.[40]

Statistical analysis

All of the results were analysed using analysis of variance (ANOVA) followed by Bonferroni post hoc tests; statistical differences were set at $p < 0.05$. With regard to biological tests, each experiment was performed at least three times in triplicate.

Results and discussion

Morphological analysis

Results obtained with SEM showed that PCL and PCL/HA scaffolds produced with the BioCell Printing had a well-defined square internal geometry, interconnected pores, with dimensions between 371 and 378 μm and a uniform spatial distribution. The extruded filaments evidenced a regular circular geometry with ~370 μm diameter, as well a good adhesion between adjacent layers (Figure 1).

Using SEM, it was also possible to evaluate qualitatively the distribution of HA particles in the filaments
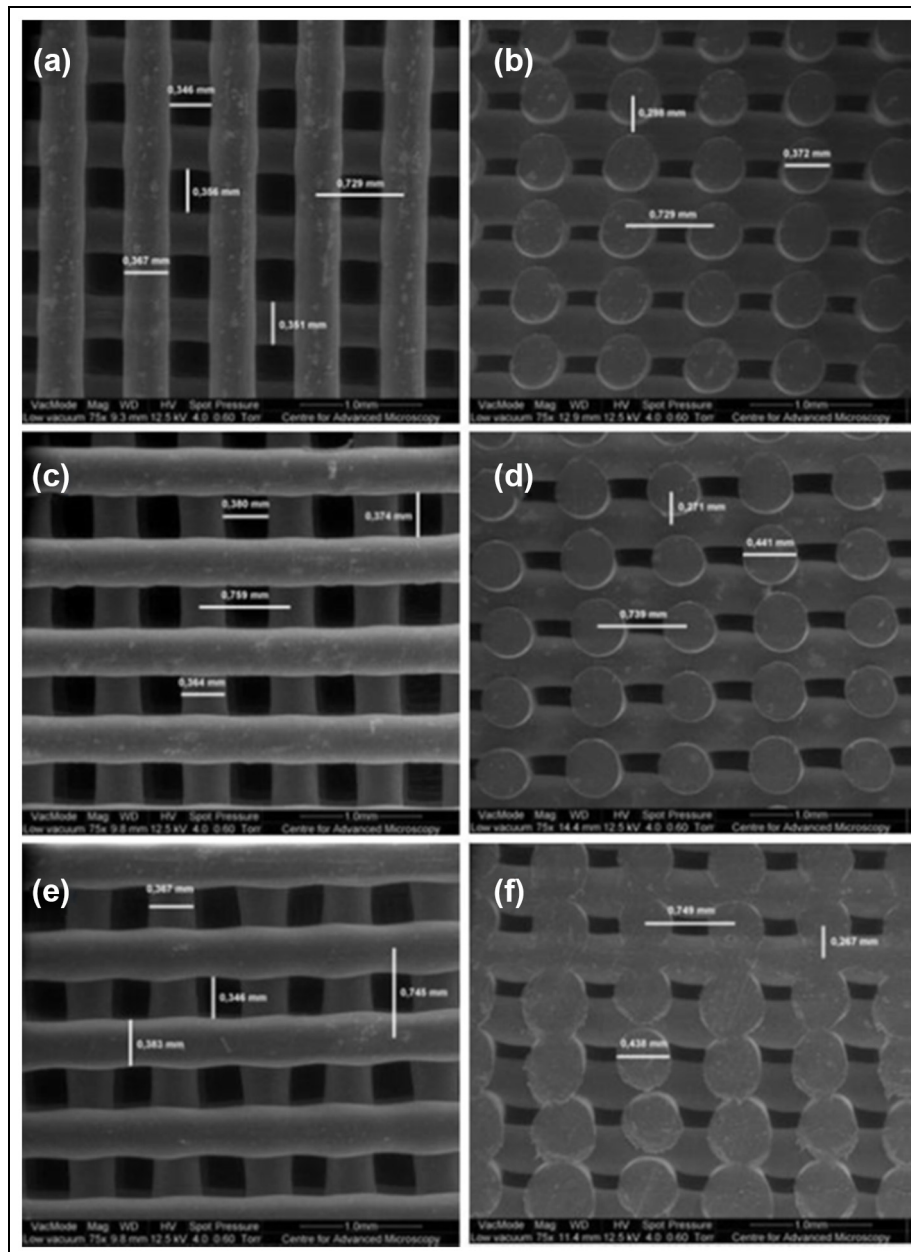

Figure 1. SEM micrographs of 3D PCL and PCL/HA scaffolds: (a) PCL top view, (b) PCL cross-section view, (c) PCL_nHA top view, (d) PCL_nHA cross-section view, (e) PCL_mHA top view and (f) PCL_mHA cross-section view.
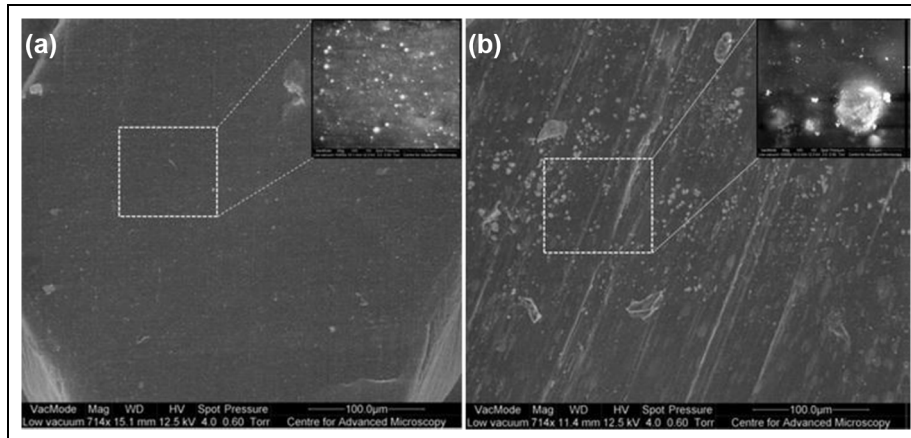
Figure 2. SEM micrographs of 3D PCL/HA filaments: (a) PCL_nHA cross-section view and (b) PCL_mHA cross-section view. Top corner amplifications of 10,000×.
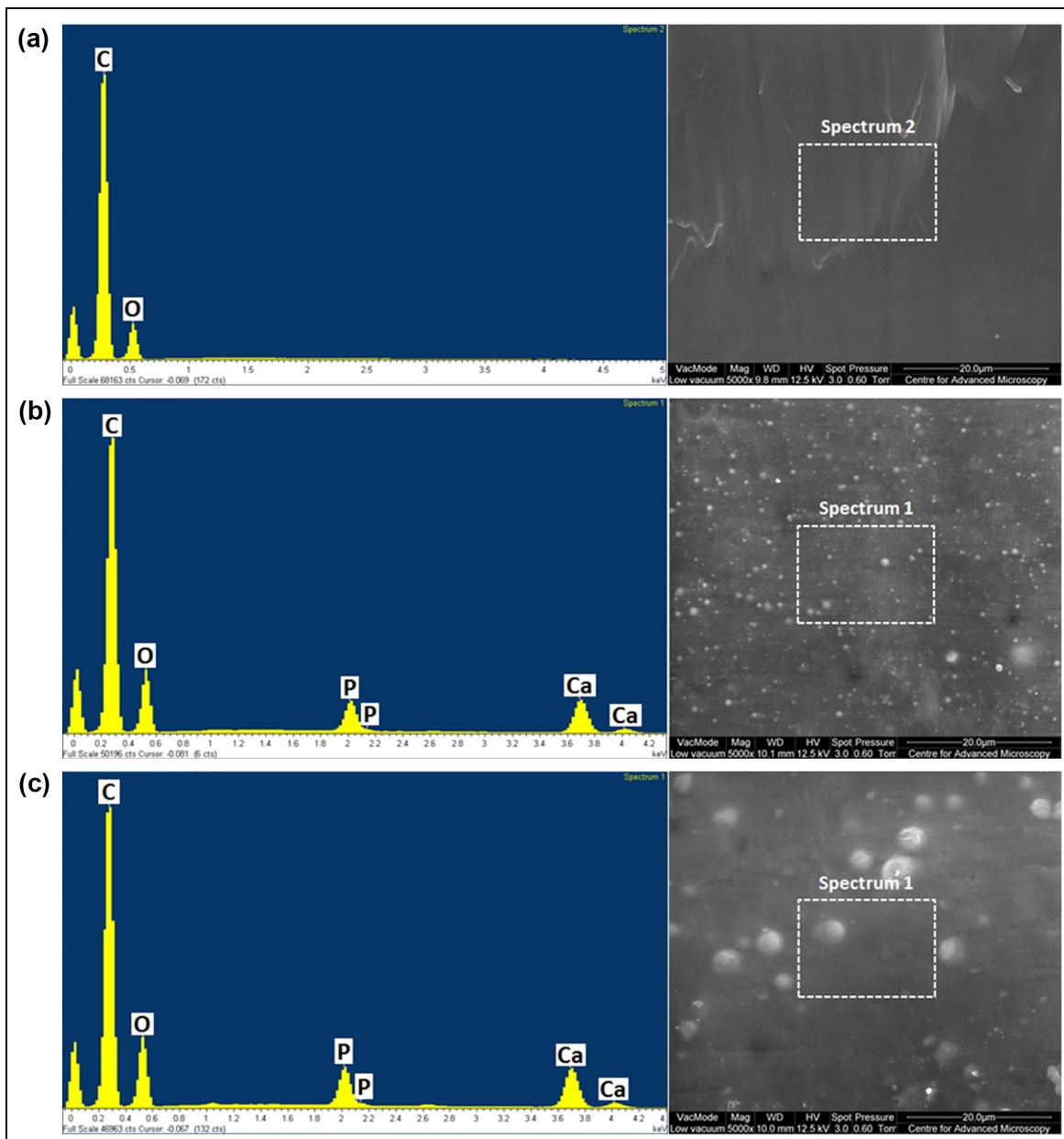
Figure 3. EDS analysis on (a) PCL scaffolds showing C and P peaks, (b) PCL_nHA scaffolds showing the peaks of Ca and P and (c) PCL_mHA scaffolds showing the peaks of Ca and P.
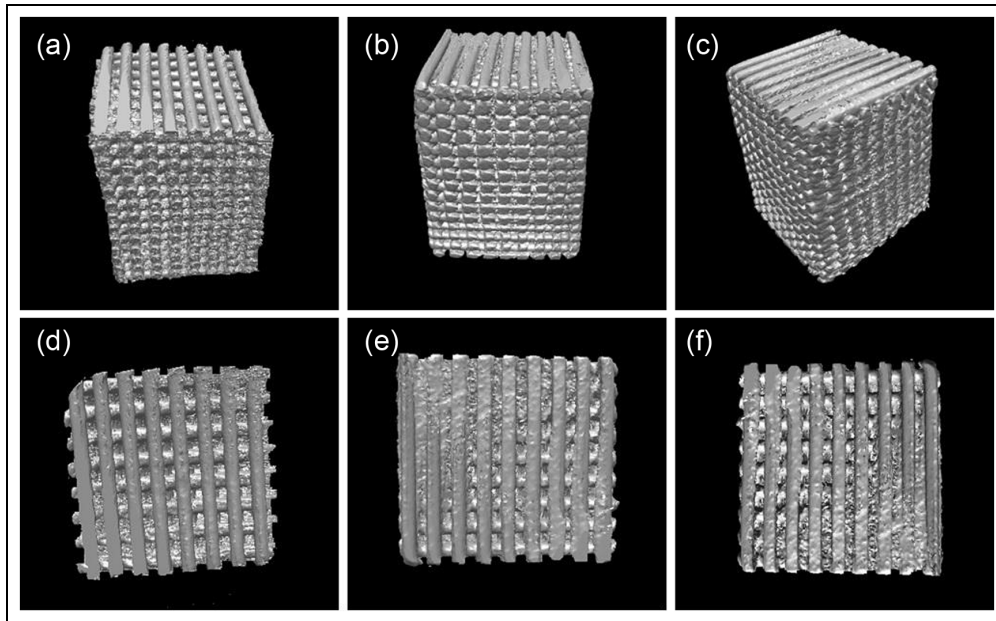
Figure 4. 3D reconstruction of PCL and PCL/HA scaffolds obtained from μCT images: (a) cross-section view of PCL scaffold, (b) cross-section view of PCL_nHA scaffold, (c) cross-section view of PCL_mHA scaffold, (d) top view of PCL scaffold, (e) top view of PCL_nHA scaffold and (f) top view of PCL_mHA scaffold.

of the scaffolds. Figure 2 clearly evidences the successful introduction of HA particles within the PCL filaments. However, from the 10,000× magnification, a much more refined and homogeneous distribution of the nHA particles is visible (Figure 2(a)) within the filaments, compared to the mHA particles (Figure 2(b)). The mHA particles should tend to form aggregates of considerably higher dimensions compared to the nHA aggregates, leading to a rough and heterogeneous distribution of HA within the PCL_mHA scaffolds.

Spectroscopy results showed the presence of HA particles in the PCL matrix, as confirmed by the HA characteristic peaks of calcium (Ca) and phosphorous (P) (Figure 3).

Through μCT analysis, it was possible to determine scaffold interconnectivity (100%), surface area to volume ratio (i.e. 20.07 mm^2/mm^3) and porosity (i.e. 58%) (Figure 4). No variations were detected between PCL, PCL_nHA and PCL_mHA scaffolds.

Mechanical analysis

Compression tests highlighted the influence of HA particles on the mechanical behaviour of the scaffolds. The obtained results were in agreement with the literature and showed that the introduction of HA increased the compressive modulus (*E*) (Figure 5; Table 2).[38,44]

The addition of 25 wt% of HA enhanced the compressive modulus of PCL scaffolds from 105.5 ± 11.2 to 138.8 ± 12.9 MPa (PCL_nHA) and 217.2 ± 21.8 MPa (PCL_mHA) as shown in Table 2. In terms of compressive modulus, the differences between 3D PCL scaffolds and PCL/HA structures, as well as those between
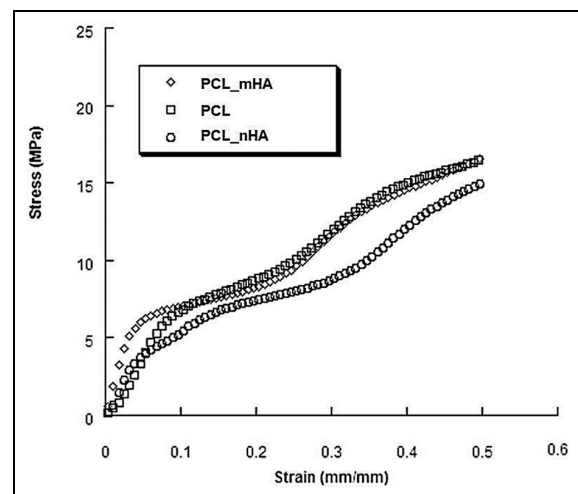
Figure 5. Typical stress–strain curves obtained for 3D PCL and PCL/HA scaffolds characterized by a 0°/90° lay-down pattern and a filament distance of 750 μm, compressed at a rate of 1 mm/min up to a strain value of 0.5 mm/mm.

PCL_nHA and PCL_mHA scaffolds, were statistically significant.

Furthermore, if compared to the neat PCL, the presence of HA particles did not significantly influence the maximum stress.

Furthermore, the results from compression tests evidenced that PCL_mHA scaffolds presented a higher value of compressive modulus than PCL_nHA scaffolds (Table 2). Such results can be ascribed to two possible reasons: (1) the heat absorption properties of the HA nanoparticles may change the crystallization process of PCL, thus altering its final mechanical

Table 2. Effect of HA particle size on the mechanical properties of PCL scaffolds.

Scaffold	Compressive modulus (E) (MPa)	Maximum stress (σ_{max}) (MPa)
PCL	105.5 ± 11.2	16.5 ± 1.4
PCL_nHA	138.8 ± 12.9	15.3 ± 1.7
PCL_mHA	217.2 ± 21.8	17.4 ± 1.8

PCL: polycaprolactone; nHA: nano-hydroxyapatite; mHA: micro-hydroxyapatite; ANOVA: analysis of variance.
Compressive modulus and maximum stress reported as mean value ± standard deviation. Statistical analysis was performed using ANOVA followed by Bonferroni post hoc tests ($p < 0.05$).
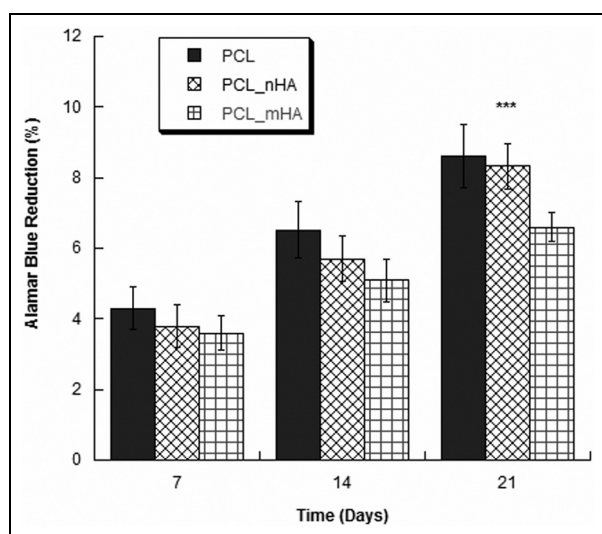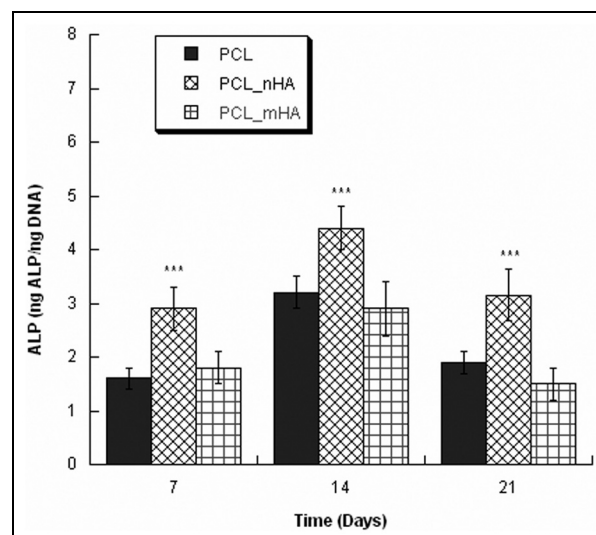

Figure 6. Percentage of Alamar Blue™ reduction as a function of time and HA granulometry. Error bar represents the standard deviation. ***$p < 0.001$ indicates statistically significant differences between PCL_nHA and PCL_mHA scaffolds, at the same time from cell seeding.

Figure 7. ALP activity as a function of time and HA granulometry. Error bar represents the standard deviation. ***$p < 0.001$ indicates statistically significant differences between PCL_nHA and PCL as well as between PCL_nHA and PCL_mHA scaffolds, at the same time from cell seeding.

properties; (2) the poor interfacial adhesion between PCL and HA particles may also have a weakening effect. This last phenomenon would be more significant in the case of PCL_nHA, where the contact area between polymer and ceramic is higher. Additional studies are being carried out to evaluate the effect of each phenomenon on the mechanical performance of the scaffolds.

Biological assay

Bone marrow–derived hMSCs were used at passages 4–6 from primary culture, as reported in the literature.[45] In vitro biological tests were performed to qualitatively and quantitatively determine the influence of HA granulometry on the biological behaviour of hMSCs. The results from the Alamar Blue assay are reported in Figure 6.

In terms of percentage of reduction of Alamar Blue, at days 7 and 14, there were no differences between PCL scaffolds and PCL-based composite structures. Furthermore, at the end of the incubation period (day 21), it was not possible to detect significant differences regarding cell viability/proliferation between PCL and PCL_nHA scaffolds. However, at day 21, PCL_nHA scaffolds presented higher cell viability when compared to PCL_mHA structures. In particular, the observed differences were statistically significant ($p < 0.001$).

As shown by SEM micrographs (Figure 2), HA micro-particles tend to form aggregates, which can act as physical barriers, preventing cells from establishing cell–cell contact and subsequent proliferation. This observation is supported by previous works,[39] where nano-HA composite scaffolds enhance the proliferation of MG-63 osteoblast-like cells.

Osteogenic differentiation was evaluated by determining the ALP activity of hMSCs. The obtained results (Figure 7) suggested that all the scaffolds were able to promote cell differentiation, independently of the presence and size of HA particles. ALP activity significantly increased during the initial stage of incubation reaching its peak at day 14. The abrupt decrease occurred between day 14 and 21 could be associated with the deposition of cell matrix (mineral phase) that inhibits the detection of ALP. In particular, PCL_nHA scaffolds showed higher levels of ALP activity compared to PCL or PCL_mHA scaffolds throughout the entire period of incubation. The observed differences were statistically significant ($p < 0.001$). Furthermore, at each time point, no differences were found between PCL and PCL_mHA. Despite its bioactive properties, all the results would seem to suggest that the presence of micro-HA particles inhibited the osteogenic differentiation of hMSCs. This should be ascribed to the potential formation of
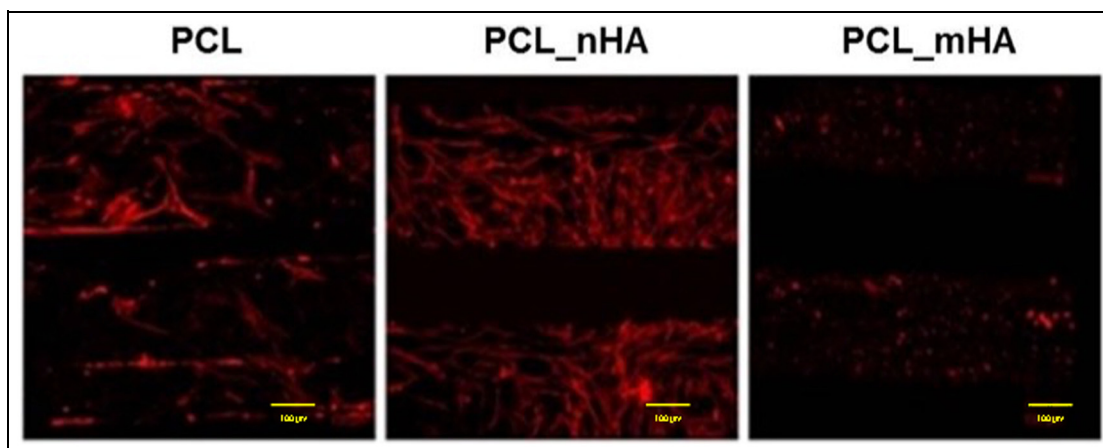
Figure 8. Typical results from CLSM analysis on PCL and PCL/HA scaffolds at day 14. Images of rhodamine phalloidin–labelled actin filaments (red).
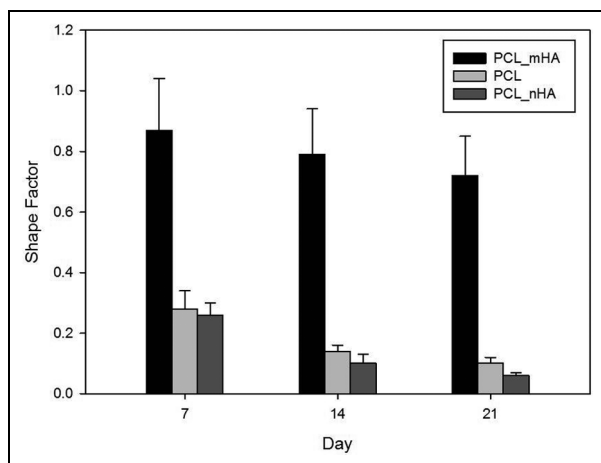
Figure 9. Typical values of shape factor obtained from CLSM images of hMSCs deposited on PCL, PCL_nHA and PCL_mHA scaffolds.

micro-HA particle aggregates on the surface of the scaffold filaments preventing the establishment of cell–cell interactions essential for the differentiation process.

Additional tests were carried in the attempt of providing a better insight into the effect of HA granulometry through the investigation of cell morphology. Confocal laser scanning microscopy (CLSM) results are depicted in Figure 8. Results at the end of 14 days of incubation showed that (1) the number of viable cells present in the PCL_nHA scaffolds was higher than PCL and PCL_mHA scaffolds (in agreement with Alamar Blue and ALP activity results); (2) cell morphology was strongly influenced by the presence and size of HA particles. With regard to PCL_nHA scaffolds, a much higher and homogeneous number of cells with filamentary morphology was present if compared to PCL and PCL_mHA scaffolds; and (3) cells adhering on PCL_mHA scaffolds presented a circular geometry showing a low degree of adhesion and few cell–cell

contact. These observations would reinforce the idea that the surface topography of PCL_mHA scaffolds prevents cellular contacts, leading to poor levels of adhesion, viability, proliferation and differentiation.

Further cell adhesion and spreading analysis were performed based on the determination of the shape factor using CLSM images. Typical values of the shape factor at 7, 14 and 21 days after cell seeding time are reported in Figure 9 as mean value ± standard deviation. Basically, the cell shape factor significantly decreased from day 7 to day 21 independently of the scaffold typology. PCL_nHA scaffolds presented the lowest shape factor at the end of the incubation period. Based on previous experiments, the lower is the cell shape factor, the more elongated is the cell.[40] Thus, the establishment of multiple cellular extensions (increased total cellular area) should imply a reduction in the shape factor (elongated cells) leading to better adhesion and spreading. These results confirmed the CLSM observations and revealed the higher potential of nano-HA to promote cell adhesion, proliferation and differentiation.

Conclusion

Composite PCL/HA scaffolds with different granulometries were successfully produced using an extrusion-based system. SEM analysis revealed composite scaffolds with square and fully interconnected pores, also providing information on the distribution of HA particles in the PCL matrix. Even though the introduction of HA enhanced the compressive modulus of the PCL structures, no statistically significant differences were found in terms of maximum stress. With regard to hMSC adhesion, proliferation and osteogenic differentiation, the biological performance of the PCL_nHA scaffolds was higher when compared to PCL_mHA scaffolds.

Acknowledgements

Declaration of conflicting interests

Funding

References

1. Lee J, Farag MM, Park EK, et al. A simultaneous process of 3D magnesium phosphate scaffold fabrication and bioactive substance loading for hard tissue regeneration. *Mater Sci Eng C Mater Biol Appl* 2014; 36: 252–260.
2. Lichte P, Pape HC, Pufe T, et al. Scaffolds for bone healing: concepts, materials and evidence. *Injury* 2011; 42: 569–573.
3. Oryan A, Alidati S, Moshiri A, et al. Bone regenerative medicine: classic options, novel strategies, and future directions. *J Orthop Surg Res* 2014; 9: 18–45.
4. Arvidson K, Abdallah BM, Applegate LA, et al. Bone regeneration and stem cells. *J Cell Mol Med* 2011; 15: 718–746.
5. Yaszemski MJ, Oldham JB, Lu L, et al. Clinical needs for bone tissue engineering technology. In: Davies JE (ed.) *Bone engineering*. Toronto, ON, Canada: University of Toronto, 2000, pp.541–547.
6. Spitzer R, Perka C, Lindenhayn K, et al. Matrix engineering for osteogenic differentiation of rabbit periosteal cells using α-tricalcium phosphate particles in a three-dimensional fibrin culture. *J Biomed Mater Res A* 2002; 59: 690–696.
7. Simon GC, Khatri CA, Wight SA, et al. Preliminary report on the biocompatibility of a moldable, resorbable, composite bone graft consisting of calcium phosphate cement and poly(lactide-co-glycolide) microspheres. *J Orthop Res* 2002; 20: 473–482.
8. Rose FR and Oreffo RO. Bone tissue engineering: hope vs hype. *Biochem Biophys Res Commun* 2002; 292: 1–7.
9. Petite H, Viateau V, Bensaid W, et al. Tissue-engineered bone regeneration. *Nat Biotechnol* 2000; 18: 959–963.
10. Perry CR. Bone repair techniques, bone graft, and bone graft substitutes. *Clin Orthop Relat Res* 1999; 360: 71–86.
11. Williams DF. Perspectives on the contributions of biomaterials and tissue engineering to bone repair, reconstruction and regeneration. In: Davies JE (ed.) *Bone engineering*. Toronto, ON, Canada: University of Toronto, 2000, pp.577–584.
12. Seto I, Asahina I, Oda M, et al. Reconstruction of the primate mandible with a combination graft of recombinant human bone morphogenetic protein-2 and bone marrow. *J Oral Maxillofac Surg* 2001; 59: 53–61.
13. Finkemeier CG. Bone-grafting and bone-graft substitutes. *J Bone Joint Surg* 2002; 84: 454–464.
14. Khan SN, Tomin E and Lane JM. Clinical applications of bone graft substitutes. *Orthop Clin North Am* 2000; 31: 389–398.
15. Melchels FPW, Domingos MAN, Klein TJ, et al. Additive manufacturing of tissues and organs. *Prog Polym Sci* 2012; 37: 1079–1104.
16. Lee SH and Shin H. Matrices and scaffolds for delivery of bioactive molecules in bone and cartilage tissue engineering. *Adv Drug Deliv Rev* 2007; 59: 339–359.
17. Anderson EJ and Tate MLK. Design of tissue engineering scaffolds as delivery devices for mechanical and mechanically modulated signals. *Tissue Eng* 2007; 13: 2525–2538.
18. Arafat MT, Lam CXF, Ekaputra AK, et al. High performance additive manufactured scaffolds for bone tissue engineering application. *Soft Matter* 2011; 7: 8013–8022.
19. Lin F, Yan C, Zheng W, et al. Preparation of mesoporous bioglass coated zirconia scaffold for bone tissue engineering. *Adv Mat Res* 2011; 365: 209–215.
20. Rath SN, Arkudas A, Lam CXF, et al. Development of a pre-vascularized 3D scaffold-hydrogel composite graft using an arterio-venous loop for tissue engineering applications. *J Biomater Appl* 2011; 27: 277–289.
21. Kolambkar YM, Dupont KM, Boerckel JD, et al. An alginate-based hybrid system for growth factor delivery in the functional repair of large bone defects. *Biomaterials* 2011; 32: 65–74.
22. Williams JM, Adewunmi A, Schek RM, et al. Bone tissue engineering using polycaprolactone scaffolds fabricated via selective laser sintering. *Biomaterials* 2005; 26: 4817–4827.
23. Cao H and Kuboyama N. A biodegradable porous composite scaffold of PGA/β-TCP for bone tissue engineering. *Bone* 2010; 46: 386–395.
24. Xiong Z, Yan Y, Zhang R, et al. Fabrication of porous poly(L-lactic acid) scaffolds for bone tissue engineering via precise extrusion. *Scripta Mater* 2001; 45: 773–779.
25. Domingos M, Chiellini F, Cometa S, et al. Evaluation of in vitro degradation of PCL scaffolds fabricated via BioExtrusion: part 1. Influence of degradation environment. *Virtual Phys Prototyp* 2010; 5: 65–73. **AQ2**
26. Patricio T, Domingos M, Gloria A, et al. Fabrication and characterisation of PCL and PCL/PLA scaffolds for tissue engineering. *Rapid Prototyping J* 2014; 2: 145–156.
27. Woodruff MA and Hutmacher DW. The return of a forgotten polymer – polycaprolactone in the 21st century. *Prog Polym Sci* 2010; 35: 1217–1256.
28. Rich J, Jaakkola T and Tirri T. In vitro evaluation of poly(ε-caprolactone-co-DL-lactide)/bioactive glass composites. *Biomaterials* 2002; 23: 2143–2150.
29. Kim HW and Jonathan C. Hydroxyapatite/PCL composite coatings on hydroxyapatite porous bone scaffold for drug delivery. *Biomaterials* 2004; 25: 1279–1287.
30. Bidic SM, Calvert JW, Marra K, et al. Rabbit calvarial wound healing by means of seeded caprotite scaffolds. *J Dent Res* 2003; 82: 131–135.
31. Fini M, Giavaresi G, Aldini NN, et al. A bone substitute composed of polymethylmethacrylate and α-tricalcium

phosphate: results in terms of osteoblast function and bone tissue formation. *Biomaterials* 2002; 23: 4523–4531.

32. Peter SJ, Lu L, Kim DJ, et al. Marrow stromal osteoblast function on a poly(propylene fumarate)/β-tricalcium phosphate biodegradable orthopaedic composite. *Biomaterials* 2000; 21: 1207–1213.

33. Hench LL and Polak JM. Third-generation biomedical materials. *Science* 2002; 295: 1014–1017.

34. Zhou Y, Hutmacher DW, Varawan SL, et al. In vitro bone engineering based on polycaprolactone and polycaprolactone–tricalcium phosphate composites. *Polym Int* 2007; 56: 333–342.

35. Schantz JT, Brandwood A, Hutmacher DW, et al. Osteogenic differentiation of mesenchymal progenitor cells in computer designed fibrin-polymer-ceramic scaffolds manufactured by fused deposition modeling. *J Mater Sci Mater Med* 2005; 16: 807–819.

36. Hong Z, Reis RL and Mano JF. Preparation and in vitro characterization of scaffolds of poly(l-lactic acid) containing bioactive glass ceramic nanoparticles. *Acta Biomater* 2008; 4: 1297–1306.

37. Douglas T, Pamula E, Hauk D, et al. Porous polymer/hydroxyapatite scaffolds: characterization and biocompatibility investigations. *J Mater Sci Mater Med* 2009; 20: 1909–1915.

38. Heo SJ, Kim SE, Wei J, et al. Fabrication and characterization of novel nano- and micro-HA/PCL composite scaffolds using a modified rapid prototyping process. *J Biomed Mater Res A* 2009; 89: 108–116.

39. Heo SJ, Kim SE, Hyun YT, et al. In vitro evaluation of poly ε-caprolactone/hydroxyapatite composite as scaffolds for bone tissue engineering with human bone marrow stromal cells. *Key Eng Mater* 2007; 342–343: 369–372.

40. Domingos M, Intranuovo F, Russo T, et al. The first systematic analysis of 3D rapid prototyped poly(ε-caprolactone) scaffolds manufactured through BioCell printing: the effect of pore size and geometry on compressive mechanical behaviour and in vitro hMSC viability. *Biofabrication* 2013; 5: 045004.

41. Bártolo P, Domingos M, Gloria A, et al. BioCell printing: integrated automated assembly system for tissue engineering constructs. *CIRP Ann: Manuf Techn* 2011; 60: 271–274.

42. Domingos M, Intranuovo F, Gloria A, et al. Improved osteoblast cell affinity on plasma-modified 3D extruded PCL scaffolds. *Acta Biomater* 2013; 9: 5997–6005.

43. Russo T, Gloria A, D-Antò V, et al. Poly(ε-caprolactone) reinforced with sol-gel synthesized organic-inorganic hybrid fillers as composite substrates for tissue engineering. *J Appl Biomater Biomech* 2010; 8: 146–152.

44. Shor L, Guçeri S, Wen X, et al. Fabrication of three-dimensional polycaprolactone/hydroxyapatite tissue scaffolds and osteoblast-scaffold interactions in vitro. *Biomaterials* 2007; 28: 5291–5297.

45. De Santis R, Russo A, Gloria A, et al. Towards the design of 3D fiber-deposited poly(ε-caprolactone)/iron-doped hydroxyapatite nanocomposite magnetic scaffolds for bone regeneration. *J Biomed Nanotechnol* 2015; 11: 1236–1246.

AQ3